

# Detection and Mass Determination of NGC 6946 from Calibrated TOBI Imaging

Demetry Alfalahat

1

February 11, 2026

## ABSTRACT

**Aims.** Estimating NGC 6946 mass and analyzing TOBi camera quality

**Methods.** NGC 6946 digital images were acquired by the TOBi telescope, which provides the flux of the galaxy for the mass estimation. The data were processed and analyzed using Python-based tools. Additional measurements were obtained from the NASA/IPAC Extragalactic Database (NED) and the Gaia Database.

**Results.**

**Conclusions.** add a git hub repository in here.

## 1. Introduction

Studying galaxies is in the heart of modern sciences. In this report, we estimated NGC 6946 mass through seven images taken by Bicocca Telescope (TOBi) which uses a Complementary Metal-Oxide-Semiconductor (CMOS) device. Four images were taken using r band ( $5500 - 7000 \text{ \AA}$ ) filter and Three using g band ( $4000 - 5500 \text{ \AA}$ ) filter<sup>1</sup>. The general framework of the report illustrates the methods followed in analyzing observational and instrumental CMOS images to estimate NGC 6946 mass.

- 10 The report is organized as follows. CMOS instrumental image analysis of TOBi telescope in Sect. 2. Sect. 3 illustrate the process of why we chose NGC 6946 galaxy for the observation. The data electron counts are calibrated to  $\text{erg}/\text{cm}^2/\text{s}$  in Sect. 4. In Sect. 5, the observational image analysis are shown and supplemented with needed codes. Finally, the mass calculations with the corresponding error are in Sect. 6 followed by the Discussion and the conclusion.
- 15 Appendix A has Python used codes (Especially for Sect. 5 as it is mostly technical) while Appendix B is for additional work and not essential for the report purpose.

## 2. CMOS Data analysis and reduction

CMOS devices introduce several sources of error. These errors arise from four main factors, which will be discussed in the data analysis section. Then, provide the general framework for dealing with these errors in the data reduction section.

### 2.1. Data analysis

- 20 A CMOS converts incoming photons into electrical charges in a two-dimensional array, which are digitized into Analog-to-Digital Units (ADU). Images taken by these semiconductors need to be calibrated by removing the manufacturing imperfections, the current produced by thermal energy, and pixel-to-pixel sensitivity variations. These three factors are

called Bias, Dark current and Flat, respectively.

The conversion of electrons into ADU introduces read-out noise (RON), which cannot be eliminated but can be characterized by the gain, measured as  $0.25 \text{ e}^-$  per ADU by the manufacturer.

Bias, dark, and flat-field frames are processed similarly: multiple exposures are averaged to produce master calibration frames (see Fig. 1).

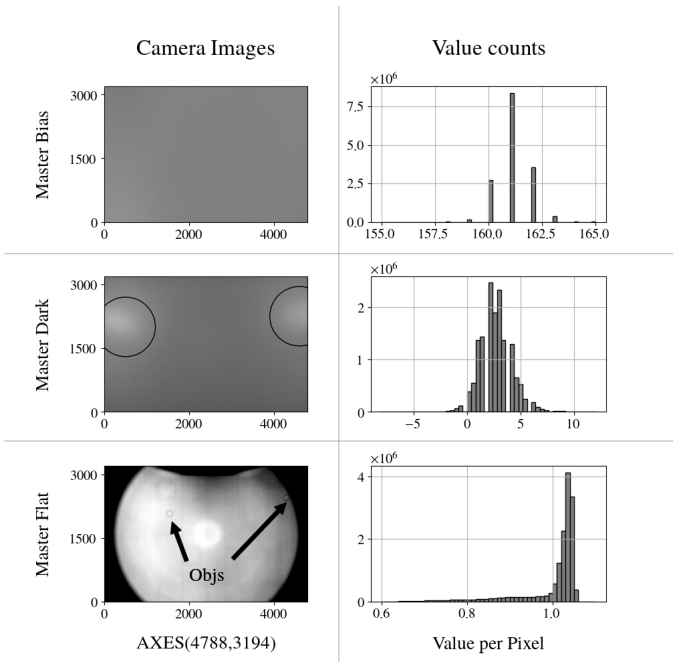


Fig. 1: Bias, Dark and Flat Frames

Bias frames are time-independent and require only averaging, while dark frames is time-dependent, which increases with longer exposures and higher temperatures. Flat frames are nor-

<sup>1</sup> There are 2 images for the i band filter but they were excluded because of the nonphysical values obtained during the mass calculation

malized to measure pixel-to-pixel sensitivity variations. The bias has been removed from the flat and dark frames<sup>2</sup> showing the exact values in the histograms. In general, the measured values are small, demonstrating the device's capability to produce high-quality images.

## 2.2. Data reduction

With the four components introduced in section 2.1, the general framework for CMOS image calibration can be expressed in Eq.1. Any CMOS image contains contributions from bias, dark current, flat-field response, and gain with the target object(Target).

$$\text{Image} = \frac{\text{Target} * \text{Flat}}{\text{Gain}} + \text{Bias} + \text{Dark} \quad (1)$$

Rearranging Eq.1 for the Target isolates the target object signal and yields in units of electrons.

## 3. Choosing appropriate target

Choosing NGC 6946 was guided by the telescope location, its capabilities, and the galaxy's luminosity. The target's coordinates ( $\text{RA} = 20^h34^m52.3236^s$ ,  $\text{Dec} = +60^\circ09'14.094''$ ) and visibility from our site were verified using online astronomical catalog and visibility tools (Ochsenbein (1996) and ING Staralt<sup>3</sup>). The final confirmation of feasibility was based on the Signal-to-Noise Ratio calculation, as discussed later.

### 3.1. Observation

Optimal imaging conditions require minimal light pollution, ideally during moonless nights with clear skies. NGC 6946 was the best choice due to it's high luminosity, face-on galaxy (inclination  $32.6^\circ$  from de Blok et al. (2008), as cited in Lara-López, M. A. et al. (2023)) and sufficient declination  $64^\circ$  where atmospheric distance is minimal.

### 3.2. Signal to Noise Ratio (SNR)

Eq.2 describes SNR, which is the source luminosity relative to the electronic and sky background noises( $N = \sqrt{(\sigma_{\text{galaxy}}^2 + \sigma_{\text{sky}}^2 + \sigma_{\text{dark}}^2 + \sigma_{\text{RON}}^2)}$ );(Raab 2012)<sup>4</sup>).This formula obeys Poisson Statistics as the Higher SNR provides better image quality.

$$\frac{S}{N} = \frac{t \cdot n_{\text{galaxy}}}{\sqrt{t \cdot n_{\text{galaxy}} + N_{\text{pix}} \cdot (n_{\text{sky}} \cdot t + n_{\text{dark}} \cdot t + N_{\text{RON}}^2)}} \quad (2)$$

The symbol names and values are defined in Table 1:

Using the r-band apparent magnitude of 7.88 for the galaxy from NASA/IPAC Extragalactic Database (NED) (2026), the calculated SNR is 9.922, which meets the observability threshold.

<sup>2</sup> Bias is included in all frames

<sup>3</sup> <https://astro.ing.iac.es/staralt/>

<sup>4</sup> <http://www.astrometrica.at/Papers/PointSources.pdf>

Table 1: Symbols and values used in the SNR calculation.

Symbol	Description	Value
$t$	Exposure time [s]	300
$n_{\text{galaxy}}$	NGC 6946 AB [ $e^- s^{-1}$ ]	33036
$n_{\text{sky}}$	Sky background [ $e^- \text{ pix}^{-1} s^{-1}$ ]	3
$n_{\text{dark}}$	Dark current [ $e^- \text{ pix}^{-1} s^{-1}$ ]	5156
$N_{\text{RON}}$	Read-out noise [ $e^- \text{ pix}^{-1}$ ]	1.5
$N_{\text{pix}}$	CCD total number of pixels	2578133

## 4. Calibration constant (C)

Physical fluxes are expressed in units of  $\text{erg cm}^{-2} \text{s}^{-1}$ . To convert the instrumental measurements (Target in Eq.1) into these physical units, a calibration constant C must be determined. This constant accounts for the telescope's filter response and is obtained by comparing the instrumental flux (IF) of a reference star in the target image with its physical flux (PF) provided by Gaia Collaboration et al. (2023). C is defined as:

$$[C] = \frac{[\text{PF}]}{[\text{IF}]} = \frac{\text{erg/cm}^2/\text{s}}{e^-} \quad (3)$$

which can be used directly:  $[\text{Flux}] = [\text{Target} \cdot C] = \text{erg/cm}^2/\text{s}$ .

The chosen star has an intermediate to low brightness, avoiding incorrect measures for over-saturated stars. It is also isolated from nearby bright sources, providing optimal conditions for extracting the sky background (see Fig.2.a). Obtaining the IF requires evaluating the integrated flux (see Fig.2.b; Appendix A.1) of the star for each of the seven images.

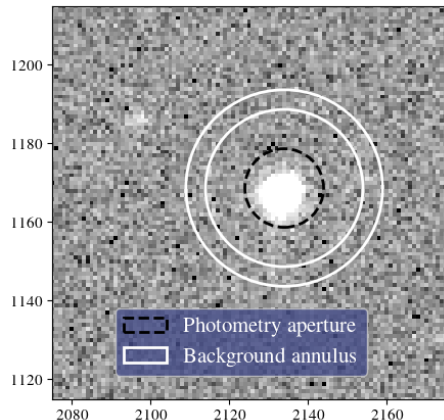


Fig. 2: a. GAIA3\_2194501 930600946944 star

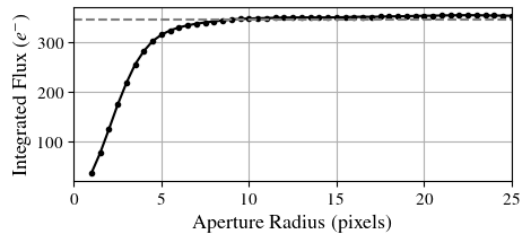


Fig. 2: b. The corresponding curve of growth

The PF of the star obtained from Gaia is calibrated with TOBI

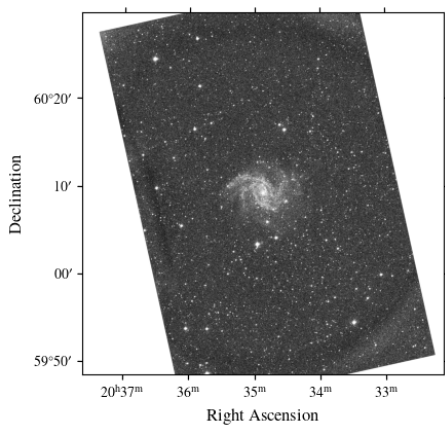


Fig. 3: Re-projected image

telescope filters through Eq.4:

$$\langle PF \rangle = \frac{\int PF \cdot QE d\lambda}{\int QE d\lambda} \quad (4)$$

Where QE is the filter quantum efficiency.

We concluded with the mean values for C, which are  $5.34 \times 10^{-17}$  and  $5.47 \times 10^{-17}$  for g and r filters in  $\text{erg cm}^{-2} \text{s}^{-1}/e^-$ .

## 5. Cleaned and Combined images: Raw Galaxy

In the previous steps, we analyzed and corrected the instrumental contributions of the data. We now focus on the astrophysical and observational components present in the calibrated science images. A raw image of the target can be schematically expressed as:

$$\text{Target} = \text{Galaxy} + \text{Stars} + \text{Sky} + \text{Rotation}$$

Here, NGC 6946 (*Galaxy*) is our main goal, separated from us by the Milky Way stars, atmospheric sky background, and the effect of Earth's rotation around itself during the exposure.

### 5.1. Sky subtraction

First, outlier values in the target image were removed by subtracting the median of the data. Then, bright sources -stars and NGC 6946- were masked to ensure an accurate measurement of the sky background. Stars were extracted using `sep.extract` code while the galaxy was masked manually. Finally, using `sep.Background` code, the sky background (bkg) variation was evaluated and subtracted from the target image (Appendix A.2).

### 5.2. Image re-projection (Rotation)

Images were taken with 20-minute exposures, resulting in slightly different galaxy positions in each frame. To align all frames to a common coordinate system centered on the galaxy, a new coordinate grid was constructed using the WCS code based on the original image coordinates. The `reproject_interp` code was then applied to transform the original galaxy coordinates into the new WCS frame (see Fig.3 ; Appendix A.3).

### 5.3. Milky Way stars

After combining all re-projected images, the radial profile `RadialProfile` of the galaxy revealed distortions in the flux

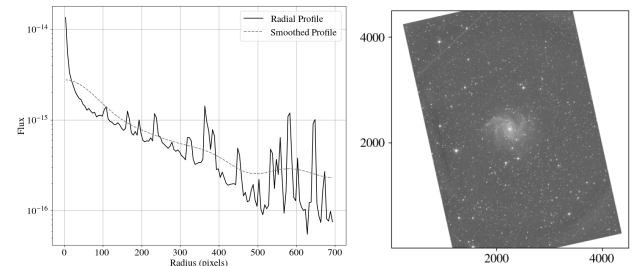


Fig. 4: a. Before masking

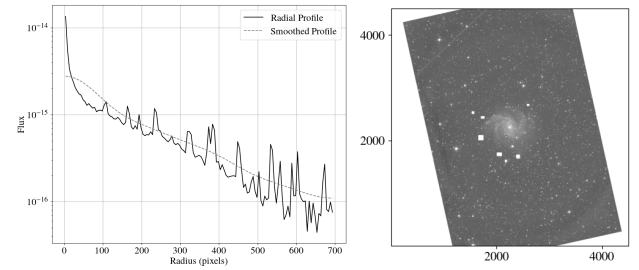


Fig. 4: b. After masking

at different radii (see Fig.4.a ; Appendix A.4). These distortions are caused by foreground Milky Way stars, which were masked manually in Fig.4.b to isolate the galaxy signal introducing the raw data of NGC 6946.

## 6. Error & Mass Estimation

140

The raw data obtained from section 5 enables the calculation of the flux measurement error and the mass of NGC 6946. The procedures applied to evaluate the error and mass based on the galaxy's integrated flux ( $\sum f_\lambda$ ; Appendix A.1). The attenuation is corrected using Balmer Decrement technique (Osterbrock & Ferland 2006) which employs the intrinsic hydrogen emission as a reference, while dust attenuation reduces the observed flux according to Eq.5 (Calzetti et al. 2000). The resultant flux ( $f_\lambda$ ) values are  $1.3 \times 10^{-8}$  and  $3.35 \times 10^{-8}$  for r and g filters in  $\text{erg/cm}^2/\text{s}$ .

$$A_\lambda = 2.5 \log_{10}\left(\frac{f_\lambda}{\sum f_\lambda}\right) = C_a \times 1.97 \log_{10}\left(\frac{H_\alpha/H_\beta}{2.86}\right) \quad (5)$$

$C_a$  is the Calzetti attenuation coefficient. The emission ratio ( $H_\alpha/H_\beta = 11.053$ ) was measured from the WHT/ISIS spectrum of the nucleus of NGC 6946 (Isaac Newton Group of Telescopes 2026).

### 6.1. Error Estimation

The total flux error  $\sigma_{f_\lambda}$  (Eq.6) is dominated by Poisson noises ( $\sigma_P$ ) and the sky background<sup>5</sup> noises ( $\sigma_{bkg}$ ):

$$\sigma_{f_\lambda} = \sqrt{\sigma_P^2 + \sigma_{bkg}^2} \quad (6)$$

$$\sigma_P = \sqrt{\frac{C \cdot f_\lambda}{t_{exp} \cdot N_{exp}}} \quad ; \quad \sigma_{bkg} = \sqrt{N_{pix}} \cdot (bkg)_{std}$$

The resulting errors are summarized in Table 2.

<sup>5</sup>  $(bkg)_{std}$  is the standard deviation of bkg obtained from `sep.Background` applied on the data obtained in section 5.

Table 2: Error values

Filter	$\sigma_P$	$\sigma_{bkg}$	$\sigma_{f_i}$
g	$4.505 \times 10^{-14}$	$1.171 \times 10^{-11}$	$1.171 \times 10^{-11}$
r	$2.446 \times 10^{-14}$	$3.477 \times 10^{-12}$	$3.477 \times 10^{-12}$

Table 3: The Estimated Mass

Filter	$C_a$	$A_\lambda$	$M_\lambda(M_\odot)$
r	$0.44 \times 3.52$	4.125	$(2.04 \pm 0.003) \times 10^{10}$
g	$0.44 \times 4.69$	5.496	$(4.43 \pm 0.006) \times 10^{10}$

## 6.2. Mass Estimation

The stellar mass is estimated using SDSS color-dependent mass-to-light ratio (Eq.7) calibrations of (Bell et al. 2003):

$$\log_{10} \frac{M_\lambda}{L_\lambda} \left[ \frac{M_\odot}{L_\odot} \right] = a_\lambda + b_\lambda \cdot \text{Color} \quad (7)$$

$$\text{Color} = -2.5 \log_{10} \frac{f_g}{f_r} \quad ; \quad L_\lambda = f_\lambda \cdot \text{Area}$$

The mass error ( $\sigma_M$ ) is evaluated through Eq.8:

$$\frac{\sigma_M}{M_\lambda} = \sqrt{\left( \frac{\sigma_{f_\lambda}}{f_\lambda} \right)^2 + (2.5 \times b_\lambda)^2 \cdot \left[ \left( \frac{\sigma_{f_g}}{f_g} \right)^2 + \left( \frac{\sigma_{f_r}}{f_r} \right)^2 \right]} \quad (8)$$

The adopted and resulting quantities in the mass calculation are summarized in Table 3.

## 7. Discussion

In this section, I will illustrate four main points to discuss the evaluated data and provide suggestions for future work. First, NGC 6946 mass values from de Blok et al. (2008) ( $(3.8 - 5.9) \times 10^{10} M_\odot$ ) and  $1.8 \times 10^{10} M_\odot$  Jarrett et al. (2019) as cited in Lara-López, M. A. et al. (2023) give a positive indication of the accuracy of the measurement and the analysis compared to Table 3. Although, the mass errors are underestimated due to neglecting the errors in NGC 6946 distance(radius), flux attenuation and using uncorrelated parameters derivation of the error formula (Eq.8). Secondly, including the i band filter fluxes would give higher accuracy but they were excluded due to the non-physical values obtained(See Fig.B.2). Thirdly, the calibration constant is applied for only one star while it could have been averaged for multiple stars. Finally, in section 5.3, the stars extraction was done manually, while using `sep.extract` would be more accurate.

## 8. conclusions

Summarize everything in the paper for someone who won't be able to read it all.

## Acknowledgments

We would like to acknowledge Knapen et al. (2023) for providing a helpful framework for this analysis. This research made use of IPython (Pérez & Granger 2007); Numpy

(Harris et al. 2020); SciPy (Virtanen et al. 2020); Astropy (Astropy Collaboration et al. 2022); Matplotlib (Hunter 2007); Photutils (Bradley et al. 2024); SEP (Barbary 2016); Reproject (Robitaille et al. 2023); and Astroquery (Ginsburg et al. 2019).

## References

- Astropy Collaboration, Price-Whelan, A. M., Lim, S. T., et al. 2022, The Astrophysical Journal, 935, 167
- Barbary, K. 2016, Journal of Open Source Software, 1, 58
- Bell, E. F., McIntosh, D. H., Katz, N., & Weinberg, M. D. 2003, ApJS, 149, 289
- Bradley, L. et al. 2024, astropy/photutils: 1.11.0
- Calzetti, D., Armus, L., Bohlin, R. C., et al. 2000, ApJ, 533, 682
- de Blok, W. J. G., Walter, F., Brinks, E., et al. 2008, AJ, 136, 2648
- Gaia Collaboration, Vallenari, A., Brown, A. G. A., et al. 2023, A&A, 674, A1
- Ginsburg, A., Sipócz, B. M., Brasseur, C. E., et al. 2019, The Astronomical Journal, 157, 98
- Harris, C. R., Millman, K. J., van der Walt, S. J., et al. 2020, Nature, 585, 357
- Hunter, J. D. 2007, Computing in Science & Engineering, 9, 90
- Isaac Newton Group of Telescopes. 2026, WHT/ISIS Spectral Data Archive, <http://casu.ast.cam.ac.uk/casuadc/ingarch/>, data retrieved for NGC 6946
- Jarrett, T. H., Cluver, M. E., Brown, M. J. I., et al. 2019, ApJS, 245, 25
- Knapen, J. H., Chamba, N., & Black, D. 2023, A&A, 673, A65
- Lara-López, M. A., Pilyugin, L. S., Zaragoza-Cardiel, J., et al. 2023, AA, 669, A25
- NASA/IPAC Extragalactic Database (NED). 2026, NASA/IPAC Extragalactic Database, <https://ned.ipac.caltech.edu>, accessed: 2026-02-05
- Ochsenbein, F. 1996, The VizieR database of astronomical catalogues
- Osterbrock, D. E. & Ferland, G. J. 2006, Astrophysics of Gaseous Nebulae and Active Galactic Nuclei (University Science Books)
- Pérez, F. & Granger, B. E. 2007, Computing in Science & Engineering, 9, 21
- Raab, H. 2012, Astrometrica: Astrometric data reduction of CCD images, Astrophysics Source Code Library, record ascl:1203.012
- Robitaille, T. et al. 2023, reproject: v0.13.0
- Virtanen, P., Gommers, R., Oliphant, T. E., et al. 2020, Nature Methods, 17, 261

## Appendix A: Detailed codes

This appendix contains the main technical parts of the codes used. For commands illustrated in the following texts, data represents CMOS image 2D array. For the full Python Jupyter Notebooks, you can access the following link for my GitHub repository:

### A.1. Integrated Flux

230 The integrated flux is used to identify the edge of a luminous object (a star or a galaxy) and it's total flux. This code creates a list of fluxes summed over different radii. Plot the fluxes with the radius to make Fig. 2.b

```
radii = np.arange(5,800,10)
fluxes = []
for r in radii:
    aperture = CircularAperture(position, r=r)
    annulus = annulus_aperture
    phot_table = aperture_photometry(data,[aperture,
        annulus])
    aperture_sum = phot_table['aperture_sum_0'][0]
    annulus_sum = phot_table['aperture_sum_1'][0]
    bkg_per_pix = annulus_sum / annulus.area
    total_bkg = bkg_per_pix * aperture.area
    net_flux = aperture_sum - total_bkg
    fluxes.append(net_flux)
```

### A.2. Sky subtraction

```
# 1- Subtracting the median
sky_level = np.median(data)
data_subtracted = data - sky_level
# 2- Extracting luminous objects
objects, segmap = sep.extract(data, thresh = 4.9,
    segmentation_map=True)
# 3- Masking the galaxy manually
position_x , position_y = 2382 ,1622
position = (position_x,position_y)
aperture = CircularAperture(position, r=700)
mask_galaxy = aperture.to_mask(method='exact').
to_image(physical_subtracted.shape).astype(bool)
segmap |= mask_galaxy
# 4- Extracting Background using mask.
bkg_masked = sep.Background( physical_subtracted ,
    mask= segmap , fw = 20 , fh = 20 )
physical_skysub = data - bkg_masked
```

```
ref_wcs.wcs.crpix = [outsize/2.0, outsize/2.0] # Specify the center of the new image in pixels.
# set projection and units
ref_wcs.wcs.ctype = ["RA---TAN","DEC--TAN"] # it defines that your image uses RA/Dec celestial coordinates on a tangent-plane sky projection
ref_wcs.wcs.cunit = ["deg","deg"] # specify units for each axis (we want them in degrees)

ref_wcs.wcs.cd = np.array([[[-scale_deg, 0.0], [0.0,
    scale_deg]]])
print(ref_wcs.has_celestial)

# Build WCS objects from headers
wcs_in_0 = WCS(header)
shape_out = (outsize, outsize)

# reprojecting the images on the grid
data_reproj_0, footprint_0 = reproject_interp(
    (data, wcs_in_0),
    ref_wcs,
    shape_out=shape_out
)
```

### A.4. Radial Profile

The Radial Profile averages all flux values on the circumference of each aperture at each radius which transforms the 2D array into 1D but without extracting the bkg as done in Appendix A.1.

```
bkg = sep.Background(data.data.astype(np.float64))
edge_radii = np.arange(1,700, 5)
rp = RadialProfile(data, position, edge_radii,error =
    bkg.back())
smooth = gaussian_filter1d(rp.profile, sigma=12)
```

## Appendix B: Discoveries

This section shows the extra work done in the lab, like extracting data<sup>6</sup> using SQL (BPT diagram in Fig.B.1) and the galaxy mass distribution for the three filters in Fig.B.2. As we see, the i-filter data are very low. I relate this to the galaxy starburst property, which should produce higher g and r filters, although, I am not sure if there is something else in the filter or the telescope as the i band is the longest wavelength and is not attenuated as the r or g bands other researches has measured the mass of NGC 6946 with the infrared as mentioned in Sect. 7.

### A.3. Image re-projection

```
from astropy.wcs import WCS
from reproject import reproject_interp

ra_gal = 308.7179
dec_gal = 60.1539
outsize = 4500
scale_deg = 0.000153
ref_wcs = WCS(naxis=2) # this line builds a grid
    centered in the galaxy coordinates

ref_wcs.wcs.crval = [ra_gal, dec_gal] # reference
    value = center coord (deg)
```

<sup>6</sup> The data are extracted from <https://skyserver.sdss.org/dr18/MoreTools/browser>

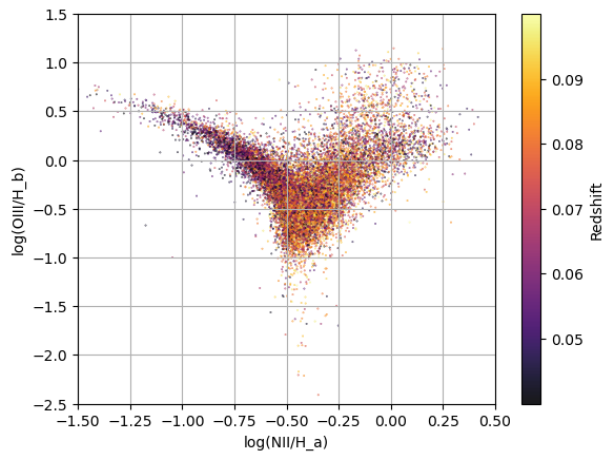


Fig. B.1: BPT diagram

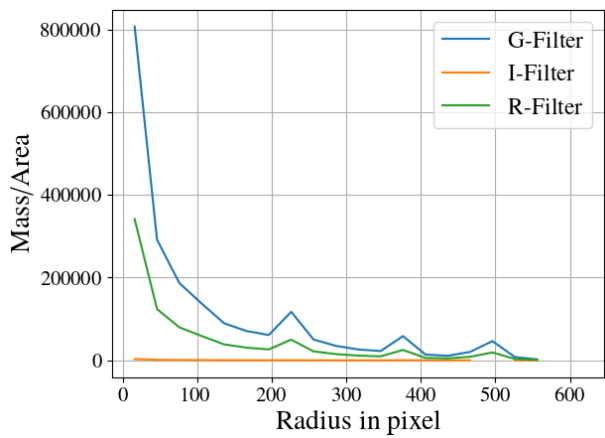


Fig. B.2: Filters comparison